Talanta 82 (2010) 85–91

Contents lists available at ScienceDirect

Talanta

journal homepage: www.elsevier.com/locate/talanta

Nonenzymatic amperometric sensor of hydrogen peroxide and glucose based on Pt nanoparticles/ordered mesoporous carbon nanocomposite

Xiangjie Bo[a], Jean Chrysostome Ndamanisha[b], Jing Bai[a], Liping Guo[a,*]

[a] Faculty of Chemistry, Northeast Normal University, Changchun 130024, PR China
[b] Université du Burundi, Institut de Pédagogie Appliquée, Bujumbura 5223, Burundi

ARTICLE INFO

Article history:
Received 25 January 2010
Received in revised form 29 March 2010
Accepted 30 March 2010
Available online 7 April 2010

Keywords:
Ordered mesoporous carbon
Platinum
Nonenzymatic
Glucose
Hydrogen peroxide

ABSTRACT

A simple and facile synthetic method to incorporate Pt nanoparticles inside the mesopores of ordered mesoporous carbons (OMCs) is reported. The Pt/OMCs nanocomposite was characterized by transmission electron microscopy (TEM), X-ray diffraction (XRD), X-ray photoelectron spectroscopy (XPS), Raman spectroscopy, and nitrogen adsorption–desorption. The results show that the incorporation of Pt nanoparticles inside the pores of OMCs does not change the highly ordered two-dimensional hexagonal mesostructure of OMCs matrix. Nonenzymatic amperometric sensor of hydrogen peroxide and glucose based on the Pt/OMCs nanocomposite-modified glassy carbon (GC) electrode is developed. Compared with the original OMCs-modified electrode, the Pt/OMCs-modified electrode displays improved current response towards hydrogen peroxide and gives linear range from 2 to 4212 μM. At an applied potential of −0.08 V, the Pt/OMCs nanocomposite gives linearity in the range of 0.5–4.5 mM glucose in neutral buffered saline solution. This glucose sensor also exhibits good ability of anti-interference to electroactive molecules. The combination the unique properties of Pt nanoparticles and the ordered mesostructure of OMCs matrix guarantees the enhanced response for hydrogen peroxide and glucose.

1. Introduction

Since the discovery of the OMCs by Ryoo et al. in 1999 [1], the particular structure of ordered mesoporous materials and their unique properties, such as periodic mesoporous structure, high specific surface area, and large pore volume, have made them very attractive materials for the design of electrochemical biosensors [2–9]. The functionalization of the surface and pores of OMCs with a variety of organic and inorganic species permits the fabrication of novel hybrid materials. A wide variety of novel methodologies used to alter the properties of OMCs have been reviewed by Stein et al. [10] and Dai and co-workers [11], respectively. Among these surface modifications, the introduction of noble metal nanoparticles further extends the applications of OMCs and provides new features such as catalytic and electrochemical activity [12–14]. There are well known methods for producing high Pt dispersions on carbon materials, but the loading amount of Pt is limited by the surface area of the carbon support and surface of the carbon matrix often must be functionalized to increase the hydrophilicity. The conventionally adopted support for Pt nanoparticles is activated carbon and carbon nanotube (CNT), which contains mostly micropores. Interior porosity is not utilized efficiently because the mass transport is very slow in these micropores. Ordered mesoporous carbon possesses periodic structure, large surface area, and high pore volume. Therefore, these materials are promising matrix for high dispersion of Pt nanomaterials [12,13,15] and accessible ordered pores can provide sufficient room for mass transport. But in those reports, the preparations of Pt nanoparticles were achieved by complicated synthetic routes. Kim and co-workers reported the preparation of Pt/OMCs catalyst by the formic acid reduction method in organic solvent tetrahydrofuran under reflux condition [16]. The problem is that organic solvent is toxic and flammable, and evaporates easily to create noxious smog. Here, we report a facile and economical route to synthesize Pt/OMCs nanocomposite via reduction of H_2PtCl_6 by formic acid in water at room temperature without polymeric stabilizers and surface functionalization. The chemically and mechanically stable 2D mesopores of OMCs can act as an ideal nanosized reactor for in situ growth of Pt nanoparticles.

Diabetes mellitus is a worldwide public health problem affecting millions of people. It is necessary to monitor the amount of blood glucose for the treatment and control of diabetes. Glucose oxidase (GOx) has been widely used in the determination of glucose. Although these biosensors based on GOx show high selectivity and sensitivity, the bioactivity of GOx is dependent on temperature and pH value due to the nature of the enzyme. To overcome the obstacle, increasing attention has been focused on the nonenzymatic glucose biosensor. Numerous nanostructured electrode materials, such as noble metals [17–24], alloys [25–30], and metal oxides [31–33],

* Corresponding author. Tel.: +86 0431 85099762; fax: +86 0431 85099762.
E-mail address: guolp078@nenu.edu.cn (L. Guo).

0039-9140/$ – see front matter © 2010 Elsevier B.V. All rights reserved.
doi:10.1016/j.talanta.2010.03.063

were developed to direct electrocatalysis of glucose. However, most of enzyme-free sensors were operated at high pH condition. Ndamanisha et al. reported nonenzymatic detection of glucose at OMCs-modified electrode in 0.1 M KOH [34]. An enzymatic glucose sensor based on Pt/OMCs was described by Zeng et al. [35]. CNTs-supported Pt or Pt-based alloy electrocatalysts were used for nonenzymatic detection of glucose [22,24,27,28,30]. But no report is found in the literature about nonenzymatic detection of glucose based on Pt/OMCs in neutral buffered saline solution. Hydrogen peroxide has wide applications in environmental, pharmaceutical, clinical, and industrial research. It is also a by-product of the reaction catalyzed by large number of oxidase enzymes. Therefore the detection of hydrogen peroxide is important in biomedical and environmental applications.

In this work, we introduce a simple method to incorporate Pt nanoparticles inside the pores of OMCs. Hydrogen peroxide and glucose was selected as marked molecule to evaluate the electrochemical activity of this new hybrid nanocomposite. The improvement of the electrocatalytic property of Pt/OMCs is observed in comparison with original OMCs.

2. Experimental

2.1. Reagents and apparatus

Pluronic P123 (non-ionic triblock copolymer, $EO_{20}PO_{70}EO_{20}$) and Nafion (5 wt%) were purchased from Sigma–Aldrich. $H_2PtCl_6{\cdot}6H_2O$ was purchased from Sinopharm Chemical Reagent Co. Ltd. All other reagents used were of analytical grade and used as received without further purification. The 0.1 M phosphate buffer saline (PBS, pH 7.3) was employed as a supporting electrolyte.

Electrochemical experiences were performed on a CHI 660C electrochemical workstation (CH Instruments, China) connected to a personal computer. A three-electrode configuration was employed, consisting of GC electrode (3 mm diameter) or a modified GC electrode serving as a working electrode, whereas an Ag/AgCl (in saturated KCl solution) and a platinum wire served as the reference and counter electrodes, respectively. XRD patterns were obtained on an X-ray D/max-2200vpc (Rigaku Corporation, Japan) instrument operated at 40 kV and 20 mA and using Cu Kα radiation (k = 0.15406 nm). Nitrogen adsorption–desorption isotherms were performed on ASAP 2020 (Micromeritics, USA). The specific surface area was calculated by the Brunauer–Emmett–Teller (BET) method. The pore size was obtained from the desorption branch of the isotherm by the Barrett–Joyner–Halenda method. The total pore volume was determined from the amount of liquid N_2 adsorbed at a relative pressure of about 0.99. TEM images were obtained using a JEM-2100F transmission electron microscope (JEOL, Japan) operating at 200 kV. XPS was measured using Thermo ESCA LAB spectrometer (USA).

2.2. Preparation of OMCs and Pt/OMCs nanocomposite

The silica template SBA-15 was synthesized using Pluronic P123 as the surfactant and tetraethyl orthosilicate as the silica source [36]. OMCs were prepared according to the method reported by Ryoo et al. [37]. The preparation of Pt/OMCs is schematically presented in Scheme 1. Pt/OMCs nanocomposite was synthesized by the following procedure: 70 mg of OMCs was dispersed in 20 mL of double distilled water containing 61.8 mg $H_2PtCl_6{\cdot}6H_2O$. After mild ultrasonication for 5 h and stirring for 1 day at room temperature, the $H_2PtCl_6{\cdot}6H_2O$ could diffuse into the pores of OMCs. Then the resultant sample was dried under vacuum to give a fine and completely dry powder. And then 10 mL double distilled water was added to redisperse the powder. 5 mL HCOOH was added to the suspension and the solution was stored at room temperature for 72 h. The product was collected and dried in an oven at 60 °C.

Approximately 60 min of ultrasonication was necessary to disperse 5 mg Pt/OMCs or OMCs into a mixture of 0.1 mL (5 wt%) Nafion and 0.9 mL distilled water. After dropping 3 μL of the suspension onto the electrode surface, the electrode was dried in air.

3. Results and discussion

3.1. Characterization of Pt/OMCs nanocomposite

The influence of incorporation of Pt nanoparticles on the mesostructure of OMCs was investigated by XRD. Fig. 1A displays the typical small-angle XRD patterns of OMCs (a) and Pt/OMCs (b). The synthesized OMCs are replicas of the parent templates SBA-15 [36], as it is evident from the presence of three XRD peaks at 2θ of 1.0°, 1.7°, and 2.0°. Partial deterioration of the ordered mesoporous structure is observed after the introduction of Pt nanoparticles. However, the existence of the main diffraction peak (1 0 0) illustrates that the framework hexagonal ordering of OMCs is basically retained after the incorporation of Pt nanoparticles. The marked intensity decrease of Pt/OMCs diffraction peaks is related to the growth of Pt nanoparticles inside the pores. The pore filling of the Pt nanoparticles can reduce the scattering contrast between the pores and the walls of the mesoporous material [38]. Fig. 1B shows the wide-angle XRD patterns of OMCs (a) and Pt/OMCs (b). Two broad diffraction peaks at 2θ of 23.4° and 44.5° are observed at

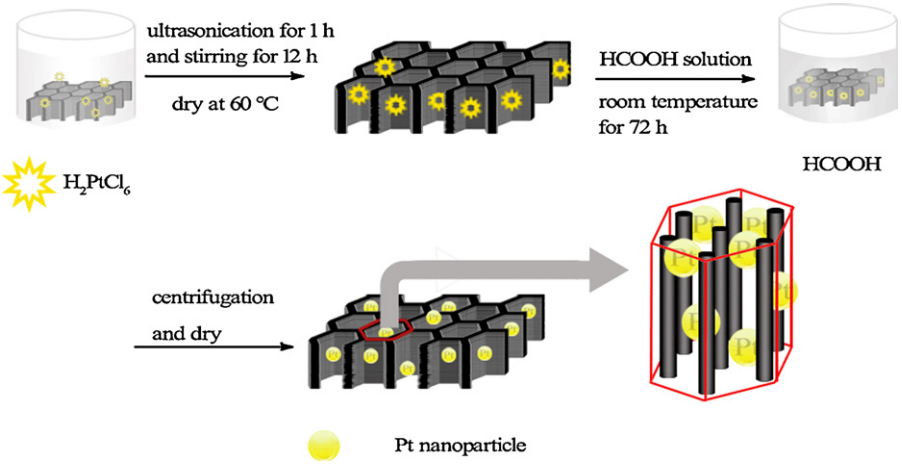

Scheme 1. Illustration of the preparation of Pt/OMCs nanocomposite.

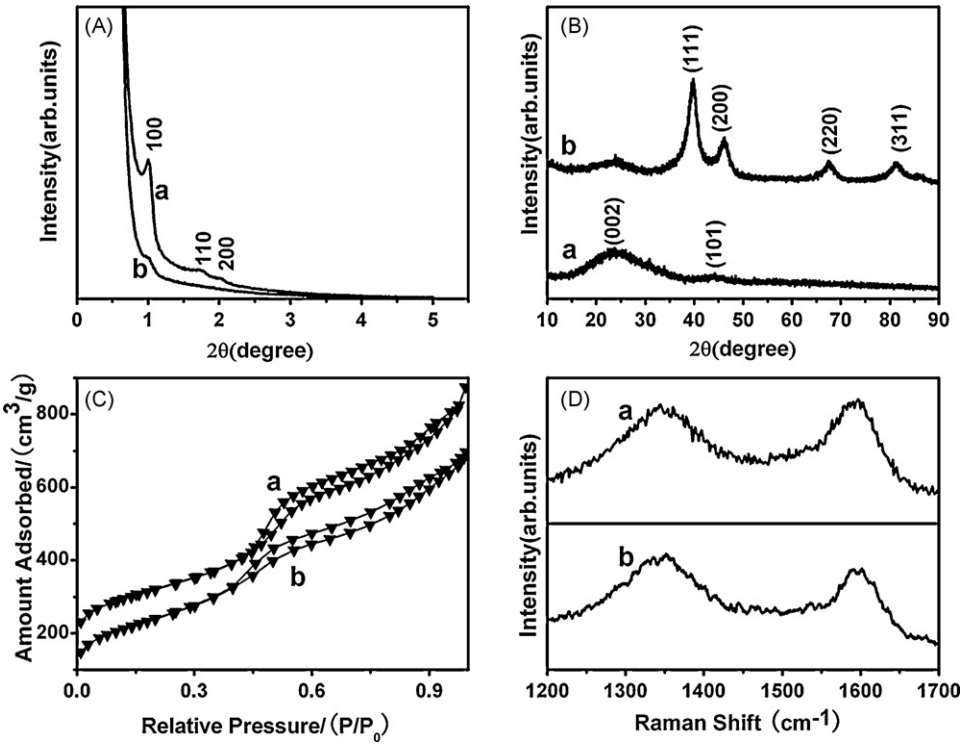

Fig. 1. (A) Small-angle XRD of (a) OMCs and (b) Pt/OMCs nanocomposite. (B) Wide-angle XRD of (a) OMCs and (b) Pt/OMCs nanocomposite. (C) Nitrogen adsorption–desorption isotherms of (a) OMCs and (b) Pt/OMCs nanocomposite. (D) Raman spectra of (a) OMCs and (b) Pt/OMCs nanocomposite.

OMCs sample, corresponding to the (0 0 2) and (1 0 1) diffractions of graphite. In the case of Pt/OMCs, several peaks appear in the wide-angle XRD pattern of Pt/OMCs nanocomposite, which can be ascribed to the characteristic peaks of Pt. This result confirms the formation of Pt/OMCs nanocomposite.

The nitrogen adsorption–desorption (Fig. 1C) was applied to investigate the change of mesostructure after the incorporation of Pt nanoparticles. The resulting sorption isotherms of OMCs (a) and Pt/OMCs (b) are characterized by type IV isotherm with some features of type I isotherm. It is observed that the isotherm changes considerably after growth of Pt nanoparticles inside the pores of OMCs. First, the adsorption capacity decreases after the incorporation of Pt nanoparticles. Second, the shift of the capillary condensation step to lower relative pressure evidences a decrease of the pore size. Table 1 shows the textural parameters of the OMCs and Pt/OMCs. The BET surface areas for OMCs and Pt/OMCs are calculated to be 1155 and 860 m^2/g, respectively. The Pt nanoparticles partially occupy the pores of OMCs and nitrogen molecules cannot access the surface of pores, and then the BET surface area of Pt/OMCs decreases compared with OMCs matrix. The total pore volumes of OMCs and Pt/OMCs are 1.72 and 1.15 cm^3/g, which also suggests that Pt nanoparticles are embedded in the pore channels of OMCs.

Raman spectroscopy was employed to study detects on the surface of the OMCs before and after functionalization. Fig. 1D presents the Raman spectra of OMCs (a) and Pt/OMCs (b). Both the spectra show the presence of D and G bands, located at 1384 cm^{-1} (disorder mode) and 1595 cm^{-1} (tangential). The D line at 1384 cm^{-1} is related to the presence of defects/disordered carbons in the graphite layer. The peak at 1595 cm^{-1} originates from the Raman active E_{2g} axial vibrational modes of the graphite sheets. Furthermore, the relative intensity ratio of the D and G bands (I_D/I_G ratio) is proportional to the number of defect sites in the graphite carbon [39]. For the OMCs and Pt/OMCs, intensity ratios I_D/I_G of 0.94 and 1.094 are observed, respectively, indicating the functionalization the pores of OMCs with Pt nanoparticles introduced more edge-plane-like defective sites existing on the surface of Pt/OMCs.

Table 1
Textural parameters of OMCs and Pt/OMCs nanocomposite.

Samples	Pore diameter (nm)	BET surface area ($m^2\ g^{-1}$)	Pore volume ($cm^3\ g^{-1}$)
OMCs	5.9	1155	1.72
Pt/OMCs	4.6	860	1.15

Fig. 2 exhibits typical TEM images of OMCs and Pt/OMCs nanocomposite. The structure of OMCs is exactly an inverse replica of their mother mold SBA-15. Fig. 2A clearly shows highly ordered carbon nanowires viewed from the [1 0 0]. Fig. 2B displays the hexagonal honeycomb-like arrangement of mesopores. Compared with the original OMCs, the pore channels are distorted to a certain degree after introduction of Pt nanoparticles (C), which reveals that Pt nanoparticles are incorporated inside the pore channels. The nanosized mesopores of OMCs can be used as nanoreactors for growth of Pt nanoparticles. It can be seen that Pt nanoparticles with size of 4 nm are uniformly dispersed in the pores of OMCs. The formation of Pt/OMCs nanocomposite was further characterized by XPS. Fig. 2D shows XPS pattern of Pt4f for Pt/OMCs nanocomposite. The Pt $4f_{7/2}$ and $4f_{5/2}$ lines appear at 71 and 74 eV, respectively, which further support the conclusion that Pt/OMCs nanocomposite have been successfully synthesized. In addition, quantitative analysis result indicates that the content of Pt is about 22.1 wt%.

3.2. Direct electrocatalysis and amperometric detection of hydrogen peroxide

Fig. 3 presents the cyclic voltammograms (CVs) of Pt/OMCs/Nafion/GC (a), OMCs/Nafion/GC (b), and Nafion/GC (c) in 0.1 M PBS (pH 7.3) in the presence 5 mM hydrogen peroxide at 50 $mV\ s^{-1}$. A reduction peak at −0.32 V is observed at OMCs/Nafion/GC electrode. The electrocatalytic activity of

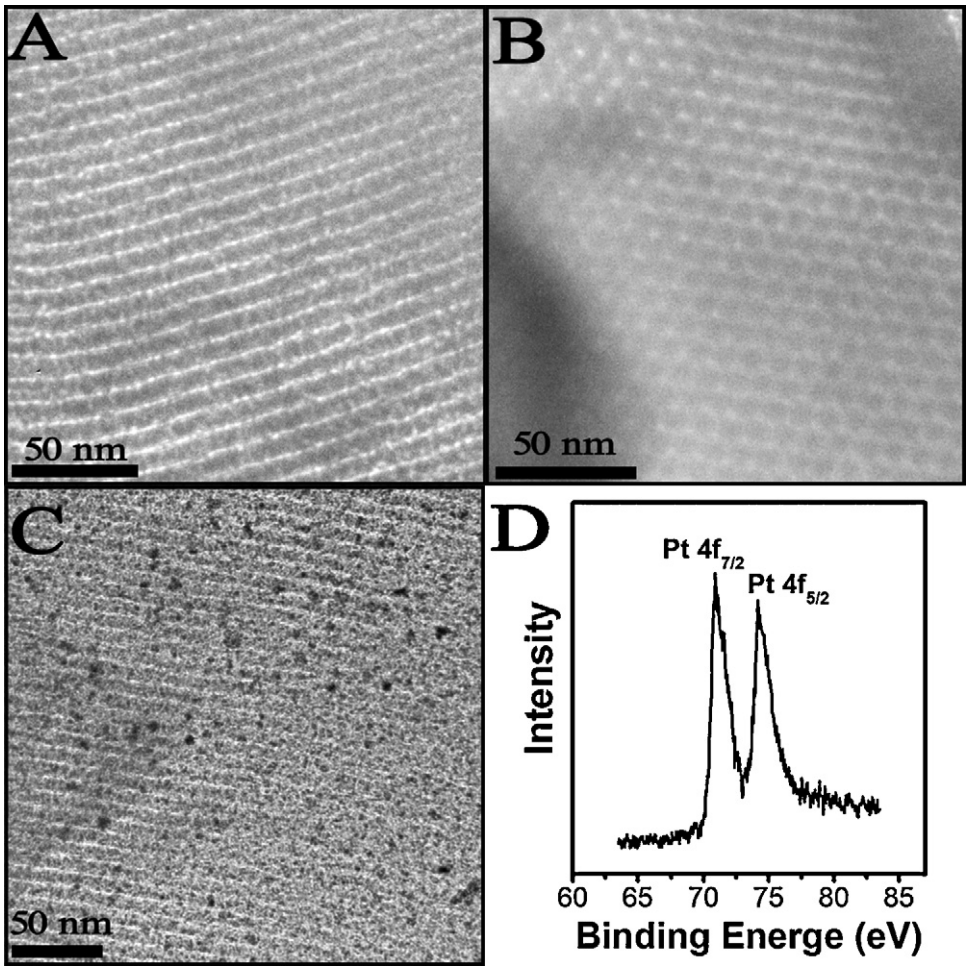

Fig. 2. (A) TEM image of OMCs viewed from [1 0 0]. (B) TEM image of OMCs viewed from [0 0 1] directions. (C) TEM images of Pt/OMCs nanocomposite. (D) XPS of Pt 4f of Pt/OMCs nanocomposite.

OMCs/Nafion/GC is ascribed to edge-plane-like defective sites on OMCs [4,5]. In the case of Pt/OMCs/Nafion/GC, the in situ attachment of Pt nanoparticles inside pores of OMCs facilitates hydrogen peroxide reduction at more positive onset reduction potential (background current was not shown) and delivers higher reduction current in comparison with original OMCs. The peak appeared at 0.06 V of Pt/OMCs/Nafion/GC is the reduction peak of the oxide of Pt [25]. The Nafion/GC exhibits a negligible response compared with Pt/OMCs/Nafion/GC. In comparison with bulk Pt electrode (d), the Pt/OMCs/Nafion/GC also exhibits an increased current signal. The negligible change of onset reduction potential between Pt/OMCs/Nafion/GC and bulk Pt electrode was also observed. The improved electrochemical response of Pt/OMCs/Nafion/GC is ascribed to the following two possible aspects. First, OMCs matrix with high specific surface area acts as a good support for achieving a high dispersion of Pt nanoparticles. Nanoscale Pt particles may supply more surface-active sites for the adsorption of reactants. Second, the ordered mesopores of OMCs can trap Pt nanoparticles while maintaining sufficient room for hydrogen peroxide molecules transport. The combination of two aspects above contributes to the enhanced current response at Pt/OMCs/Nafion/GC.

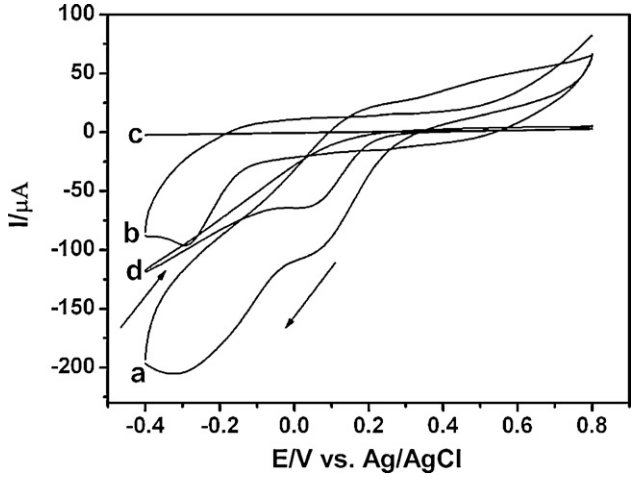

Fig. 3. CVs of (a) Pt/OMCs/Nafion/GC, (b) OMCs/Nafion/GC, (c) Nafion/GC, and (d) bulk Pt in 0.1 M PBS (pH 7.3) containing 5 mM hydrogen peroxide at 50 mV s^{-1}.

Fig. 4 shows the amperometric *i*–*t* curve of Pt/OMCs/Nafion/GC with successive additions of hydrogen peroxide at the potential of −0.10 V. The Pt/OMCs/Nafion/GC electrode has linear chronoamperometric responses to hydrogen peroxide concentrations between 2 and 4212 μM ($R = 0.998$, $n = 41$). The sensitivity is calculated as $173.4 \pm 11.2\ \mu A\ mM^{-1}\ cm^{-2}$ (the slope of calibration plot divided by geometric surface area of GC electrode). The detection limit is 1.2 μM with the signal-to-noise ratio of three. A comparison of linear range, detection limit, sensitivity, and detection potential for Pt/OMCs nanocomposite-modified electrode with other hydrogen peroxide sensors reported in the literature is

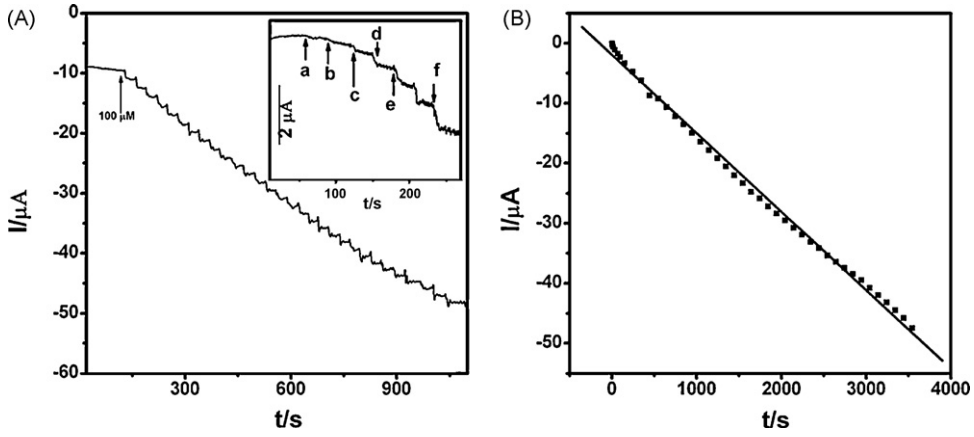

Fig. 4. (A) The amperometric *i–t* curve of Pt/OMCs/Nafion/GC with successive additions of hydrogen peroxide at the potential of −0.10 V. Inset shows the amplification of amperometric response of (a) 2 μM, (b) 4 μM, (c) 10 μM, (d) 20 μM, (e) 30 μM, and (f) 50 μM hydrogen peroxide. (B) The corresponding calibration plots for hydrogen peroxide.

shown in Table 2. All the data reveal the analytical parameters for Pt/OMCs/Nafion/GC electrode are comparable and even better than those obtained at several electrodes reported recently. Therefore, the Pt/OMCs nanocomposite is a good electrode material for preparation of low detection potential, sensitive, and wide linear range amperometric sensor for hydrogen peroxide. The reproducibility of the sensor was also investigated for five repetitive measurements with successive additions of 0.1 mM hydrogen peroxide at −0.10 V. The relative standard deviation of the sensitivity was less than 5.2%. When the Pt/OMCs/Nafion/GC electrode was stored at 4 °C for 2 weeks, the sensitivity for successive additions of 0.1 mM hydrogen peroxide at −0.10 V remained 94.6% of its original value, suggesting the long-term stability of the electrode.

3.3. Direct electrocatalysis and amperometric detection of Glucose

Fig. 5 presents the CVs obtained in 0.1 M PBS (pH 7.3) containing 0 mM (dash line) and 50 mM (solid line) glucose at OMCs/Nafion/GC, Pt/OMCs/Nafion/GC, and bulk Pt electrodes at 5 mV s^{-1}. No obvious peak corresponding to the oxidation of glucose is observed at the OMCs/Nafion/GC in the potential range studied. Multiple anodic peaks attributed to the oxidation of glucose and resulting intermediates are observed in the positive scan. The result can be explained by the well-established mechanism of electro-oxidation of glucose on Pt electrodes in neutral media [25,46]. At the low potential the first peak at 0 V could be attributed to the electrosorption of glucose forming glucose intermediates. The formed intermediates could inhibit the further electrosorption of glucose resulting in the decrease in current when increasing the electrode potential to 0.1 V. The second weak peak occurs at about 0.2 V, perhaps due to the oxidation of the intermediate layer and the partial oxidation of glucose. However, this peak is obvious at bulk Pt electrode. At potential above 0.3 V further oxidation of glucose and its intermediates may occur forming products such as gluconolactone or gluconic acid, resulting in a peak at 0.6 V. The decrease in current at more positive potential could be due to the formation of thick Pt oxide which competes for surface adsorption sites with glucose and in turn inhibits the electro-oxidation of glucose as well. In the negative scan, the oxidation of glucose is also suppressed in the high potential range because of the presence of Pt surface oxide. With the reduction of surface Pt oxide around 0.14 V, more and more surface-active sites are available for the oxidation of glucose again, resulting in an anodic peak in the potential at −0.08 V. The electrochemical characteristics of the bulk Pt electrode to the oxidation of glucose are similar to those of Pt/OMCs/Nafion/GC. However, the current is only ca. 1/7 of that obtained at the Pt/OMCs/Nafion/GC. The discrepancy of current between Pt/OMCs/Nafion/GC and bulk Pt electrode may be ascribed to the increased active surface area of nanoscale Pt particles at Pt/OMCs/Nafion/GC.

The amperometric responses of Pt/OMCs/Nafion/GC to successive additions glucose at the potential of −0.08 V is shown in Fig. 6. The current increases stepwise with each successive addition of glucose solution at the Pt/OMCs/Nafion/GC electrode. The Pt/OMCs/Nafion/GC has linear chronoamperometric responses to glucose concentrations between 0.5 and 4.5 mM. The Pt/OMCs/Nafion/GC biosensor exhibits a high sensitivity of 16.69 μA mM^{-1} cm^{-2} (the slope of calibration plot divided by geometric surface area of GC electrode), which is higher than those of

Table 2
Comparison of the performance of various hydrogen peroxide sensors.

Electrode	Linear range (μM)	Detection limit (μM) ($S/N = 3$)	Sensitivity (μA mM^{-1} cm^{-2})	Potential applied (V)	Reference
Hb/Nafion/GMC[a]/GC	1–267	1.2	101.6	−0.388 (vs. Ag/AgCl)	[40]
Ti(III)–TNTs[b]/Hb	4.9–1100	1.5	31.8	−0.10 (vs. SCE)	[41]
(PDDA[c]/Fe_3O_4)$_5$/ITO[d]	4.18–800	1.4	–	−0.20 (vs. Ag/AgCl)	[42]
HRP/Nafion/SPE[e]	5.98–35.36	0.48	143.3	−0.35 (vs. SCE)	[43]
ZnO/Au/Nafion/HRP/GC	15–1100	9	–	−0.30 (vs. Ag/AgCl)	[44]
Cu_2S/OMCs/Nafion/GC	1–3030	0.2	36.8	−0.10 (vs. Ag/AgCl)	[45]
Pt/OMCs/Nafion/GC	2–4212	1.2	173.4 ± 11.2	−0.10 (vs. Ag/AgCl)	This work

[a] Graphitized ordered macroporous carbon.
[b] TiO_2 nanotubes in situ self-doped with Ti(III).
[c] Poly(diallyldimethylammonium chloride).
[d] Tin-doped indium oxide.
[e] Screen-printed electrode.

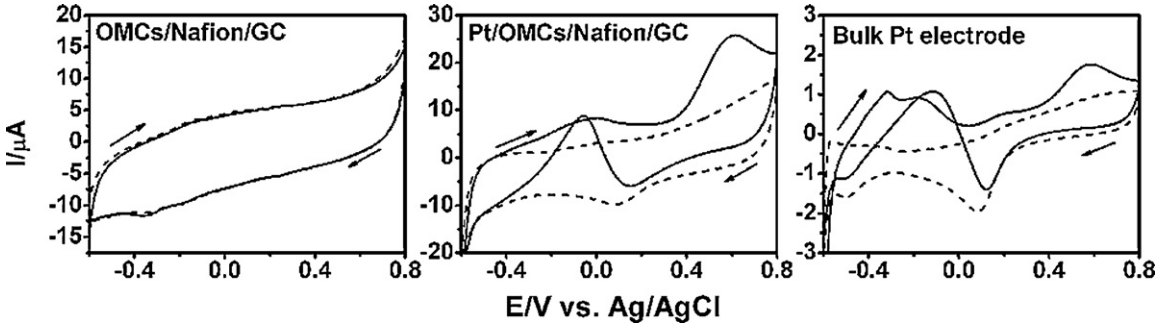

Fig. 5. CVs obtained in 0.1 M PBS (pH 7.3) containing 0 mM (dash line) and 50 mM (solid line) glucose at OMCs/Nafion/GC, Pt/OMCs/Nafion/GC, and bulk Pt electrodes at 5 mV s^{-1}.

platinum nanotubule arrays (0.1 μA mM^{-1} cm^{-2}) [17], mesoporous platinum (9.6 μA mM^{-1} cm^{-2}) [18], gold nanotube array electrode (1.13 μA mM^{-1} cm^{-2}) [19], and PtCo alloy (13.7 μA mM^{-1} cm^{-2}) [29]. The Pt/OMCs/Nafion/GC shows a detection limit of 0.13 mM (three times the signal-to-noise ratio). Compared with the Pt-based CNT hybrid electrocatalysts for nonenzymatic glucose detection in alkaline solution [23,24,30], the improved sensitivity at Pt/OMCs/Nafion/GC is contributed to the favorable diffusion passage in the mesopores and highly dispersed Pt nanoparticles in the OMCs matrix. We also investigated the interference effect of ascorbic acid, uric acid, and dopamine towards the determination of glucose at −0.08 V (inset of Fig. 6A). The Pt/OMCs/Nafion/GC produces negligible current signal for 0.1 mM ascorbic acid, 0.1 mM dopamine, and 0.1 mM uric acid. The good ability of anti-interference is attributed to the low potential. But the existence of 0.15 M chloride ions causes the decrease of 36% in the current of 50 mM glucose. This can be explained by the competitive adsorption between glucose and chloride ions [25]. The glucose molecules firstly undergo electrosorption on the electrode surface to form a layer of glucose intermediates, which can be easily oxidized. The adsorbed intermediates are oxidized at more positive potentials, forming products such as gluconolactone or gluconic acid. However, when large amounts of chloride ions are present, chloride ions compete with the adsorbing glucose intermediates and preferentially block or occupy part of active sites, causing less chance of reactive species approaching the electrode surface. Research to improve the resistance of chloride poisoning is currently doing in our laboratory. When the Pt/OMCs/Nafion/GC electrode was stored at 4 °C for 2 weeks, the current response to 50 mM glucose remained 93.2% of its original value, suggesting the long-term stability of the electrode. The reproducibility of the sensor was also investigated. The relative standard deviation for 50 mM glucose sensing was less than 7.4% for five measurements for the same electrode.

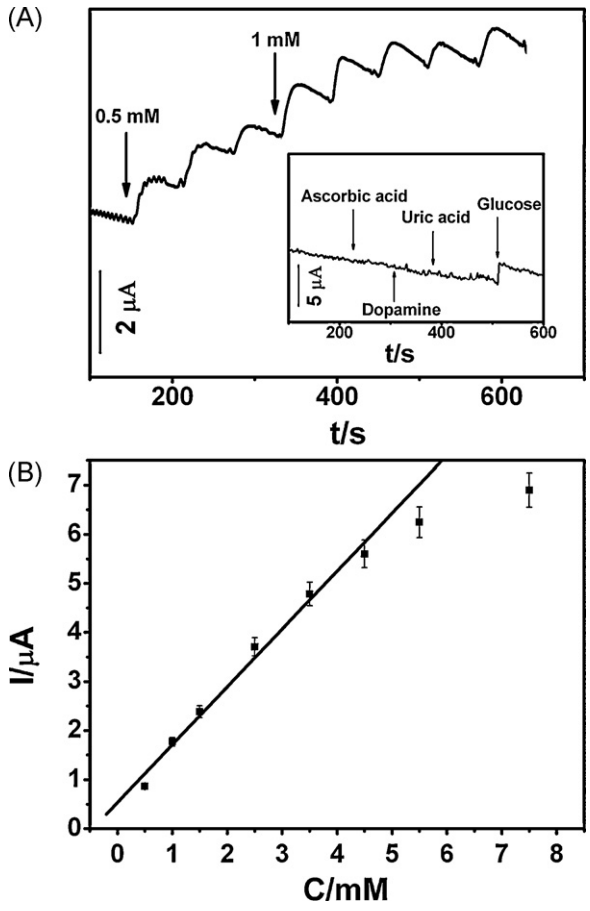

Fig. 6. (A) The amperometric *i–t* curve of Pt/OMCs/Nafion/GC with successive additions of glucose at the potential of −0.08 V. Inset shows the amperometric *i–t* curve of Pt/OMCs/Nafion/GC to successive additions of 0.1 mM ascorbic acid, 0.1 mM dopamine, 0.1 mM uric acid and 1 mM glucose at −0.08 V. (B) The corresponding calibration plots for glucose.

4. Conclusion

A facile and simple method has been developed to synthesize Pt/OMCs nanocomposite with Pt nanoparticles embedded inside the mesopores of OMCs matrix. Although deterioration of the ordered structure was observed after incorporation of the Pt nanoparticles, the Pt/OMCs nanocomposite exhibits improved electrochemical response towards hydrogen peroxide and glucose compared to original OMCs. The combination the unique properties of Pt nanoparticles and the ordered mesostructure of OMCs matrix endows Pt/OMCs nanocomposite as an ideal candidate for nonenzymatic detection of hydrogen peroxide and glucose.

Acknowledgements

The authors gratefully acknowledge the financial support by the National Natural Science Foundation of China (No. 20875012).

References

[1] R. Ryoo, S.H. Joo, S. Jun, J. Phys. Chem. B 103 (1999) 7743–7746.
[2] M. Zhou, J. Ding, L.P. Guo, Q.K. Shang, Anal. Chem. 79 (2007) 5328–5335.
[3] G. Hu, Y. Guo, S. Shao, Biosens. Bioelectron. 24 (2009) 3391–3394.
[4] N. Jia, Z. Wang, G. Yang, H. Shen, L. Zhu, Electrochem. Commun. 9 (2007) 233–238.
[5] M. Zhou, L. Shang, B. Li, L. Huang, S. Dong, Electrochem. Commun. 10 (2008) 859–863.
[6] J.C. Ndamanisha, J. Bai, B. Qi, L. Guo, Anal. Biochem. 386 (2009) 79–84.
[7] L. Zhu, C. Tian, D. Yang, X. Jiang, R. Yang, Electroanalysis 20 (2008) 2518–2525.
[8] C. You, X. Xu, B. Tian, J. Kong, D. Zhao, B. Liu, Talanta 78 (2009) 705–710.
[9] D. Zheng, J. Ye, L. Zhou, Y. Zhang, C. Yu, J. Electroanal. Chem. 625 (2009) 82–87.

[10] A. Stein, Z. Wang, M.A. Fierke, Adv. Mater. 21 (2009) 265–293.
[11] C. Liang, Z. Li, S. Dai, Angew. Chem. Int. Ed. 47 (2008) 3696–3717.
[12] S.H. Joo, S.J. Choi, I. Oh, J. Kwak, Z. Liu, O. Terasaki, R. Ryoo, Nature 412 (2001) 169–172.
[13] W.C. Choi, S.I. Woo, M.K. Jeon, J.M. Sohn, M.R. Kim, H.J. Jeon, Adv. Mater. (2005) 446–451.
[14] T. Harada, S. Ikeda, M. Miyazaki, T. Sakata, H. Mori, M. Matsumura, J. Mol. Catal. A: Chem. 268 (2007) 59–64.
[15] Y. Sun, L. Zhuang, J. Lu, X. Hong, P. Liu, J. Am. Chem. Soc. 129 (2007) 15465–15467.
[16] Y. Jung, S. Kim, S.-J. Park, J.M. Kim, Colloids Surf. A: Physicochem. Eng. Aspects 313–314 (2008) 167–170.
[17] J. Yuan, K. Wang, X. Xia, Adv. Funct. Mater. 15 (2005) 803–809.
[18] S. Park, T.D. Chung, H.C. Kim, Anal. Chem. 75 (2003) 3046–3049.
[19] Y.-G. Zhou, S. Yang, Q.-Y. Qian, X.-H. Xia, Electrochem. Commun. 11 (2009) 216–219.
[20] Y. Bai, W. Yang, Y. Sun, C. Sun, Sens. Actuators B 134 (2008) 471–476.
[21] H. Zhu, X. Lu, M. Li, Y. Shao, Z. Zhu, Talanta 79 (2009) 1446–1453.
[22] D. Rathod, C. Dickinson, D. Egan, E. Dempsey, Sens. Actuators B 143 (2010) 547–554.
[23] L.Q. Rong, C. Yang, Q.Y. Qian, X.H. Xia, Talanta 72 (2007) 819–824.
[24] L.H. Li, W.D. Zhang, Microchim. Acta 163 (2008) 305–311.
[25] J. Wang, D.F. Thomas, A. Chen, Anal. Chem. 80 (2008) 997–1004.
[26] P. Holt-Hindle, S. Nigro, M. Asmussen, A. Chen, Electrochem. Commun. 10 (2008) 1438–1441.
[27] H.-F. Cui, J.-S. Ye, W.-D. Zhang, C.-M. Li, J.H.T. Luong, F.-S. Sheu, Anal. Chim. Acta 594 (2007) 175–183.
[28] F. Xiao, F. Zhao, D. Mei, Z. Mo, B. Zeng, Biosens. Bioelectron. 24 (2009) 3481–3486.
[29] F. Zhao, F. Xiao, B. Zeng, Electrochem. Commun. 12 (2010) 168–171.
[30] L.H. Li, W.D. Zhang, J.S. Ye, Electroanalysis 20 (2008) 2212–2216.
[31] J. Chen, W.D. Zhang, J.S. Ye, Electrochem. Commun. 10 (2008) 1268–1271.
[32] Z. Zhuang, X. Su, H. Yuan, Q. Sun, D. Xiao, M.M.F. Choi, Analyst 133 (2008) 126–132.
[33] S. Cherevko, C.-H. Chung, Talanta 80 (2010) 1371–1377.
[34] J.C. Ndamanisha, L. Guo, Bioelectrochemistry 77 (2009) 60–63.
[35] J. Yu, D. Yu, T. Zhao, B. Zeng, Talanta 74 (2008) 1586–1591.
[36] D. Zhao, J. Feng, Q. Huo, N. Melosh, G.H. Fredrickson, B.F. Chmelka, G.D. Stucky, Science 279 (1998) 548–552.
[37] S. Jun, S.H. Joo, R. Ryoo, M. Kruk, M. Jaroniec, Z. Liu, T. Ohsuna, O. Terasaki, J. Am. Chem. Soc. 122 (2000) 10712–10713.
[38] B. Marler, U. Oberhagemann, S. Vortmann, H. Gies, Microporous Mater. 6 (1996) 375–383.
[39] V. Georgakilas, D. Voulgaris, E. Vázquez, M. Prato, D.M. Guldi, A. Kukovecz, H. Kuzmany, J. Am. Chem. Soc. 124 (2002) 14318–14319.
[40] X. Lu, Y. Xiao, Z. Lei, J. Chen, Biosens. Bioelectron. 25 (2009) 244–247.
[41] M. Liu, G. Zhao, K. Zhao, X. Tong, Y. Tang, Electrochem. Commun. 11 (2009) 1397–1400.
[42] L. Zhang, Y. Zhai, N. Gao, D. Wen, S. Dong, Electrochem. Commun. 10 (2008) 1524–1526.
[43] Y.J. Teng, S.H. Zuo, M.B. Lan, Biosens. Bioelectron. 24 (2009) 1353–1357.
[44] C. Xiang, Y. Zou, L.-X. Sun, F. Xu, Sens. Actuators B 136 (2009) 158–162.
[45] X. Bo, J. Bai, L. Wang, L. Guo, Talanta 81 (2010) 339–345.
[46] S. Ernst, J. Heitbaum, C.H. Hamann, J. Electroanal. Chem. 100 (1979) 173–183.